

# The properties of long gamma-ray bursts in massive compact binaries

Ross P. Church<sup>1\*</sup>, Chunglee Kim<sup>2,1</sup>, Andrew J. Levan<sup>3</sup> and Melvyn B. Davies<sup>1</sup>

<sup>1</sup>*Lund Observatory, Department of Astronomy and Theoretical Physics, Box 43, SE-221 00, Lund, Sweden.*

<sup>2</sup>*Department of Physics, West Virginia University, Morgantown, WV 26506, USA.*

<sup>3</sup>*Department of Physics, University of Warwick, Coventry, CV4 7AL*

Accepted 2012 XXXber XX . Received 2012 XXXber XX; in original form 2012 October XX

## ABSTRACT

We consider a popular model for long-duration gamma-ray bursts, in which the progenitor star, a stripped helium core, is spun up by tidal interactions with a black-hole companion in a compact binary. We perform population synthesis calculations to produce a representative sample of such binaries, and model the effect that the companion has on material that falls back on to the newly-formed black hole. Taking the results of hydrodynamic models of black-hole formation by fallback as our starting point, we show that the companion has two principal effects on the fallback process. First, a break forms in the accretion curve at around  $10^4$  s. Secondly, subsequent to the break, we expect to see a flare of total energy around  $10^{50}$  erg. We show that the break and flare times are set largely by the semi-major axis of the binary at the time of explosion, and that this correlates negatively with the flare energy. Although comparison with observations is non-trivial, we show that our predicted break times are comparable to those found in the X-ray light curves of canonical long-duration gamma-ray bursts. Similarly, the flare properties that we predict are consistent with the late-time flares observed in a sub-sample of bursts.

**Key words:** Stars: gamma-ray burst: general; stars: binaries: close; stars: evolution; stars: supernova: general

## 1 INTRODUCTION

The launch of the *Swift* satellite in 2004 has provided a massive step forwards in our ability to observe gamma-ray bursts, in particular at early times (Gehrels et al. 2004). The combination of rapid triggering and localisation with panoramic follow-up has provided a large and growing sample of burst light-curves and spectra with which to confront theoretical models. Using this data, theoretical work continues to elucidate the progenitors of gamma-ray bursts. In this paper we focus on long gamma-ray bursts (LGRBs), for which the model of Woosley (1993) has stood up well to the last two decades of observations. This posits the origin of LGRBs as accretion of a stellar-mass quantity of material from an angular-momentum-supported disc around a newly-formed stellar-mass black hole. This model is supported by strong observational evidence for an association between LGRBs and type Ib/c supernovae (Stanek et al. 2003); for a recent review of the evidence see Hjorth & Bloom (2011).

The specific rates of gamma-ray bursts, even once corrected for a narrow beaming angle, are consistent with them forming from a small fraction of type Ib/c supernovae (Podsiadlowski et al. 2004).

The main theoretical problem with this scenario is that a rapid rate of stellar rotation is needed at the moment of core collapse, in order to endow the core with sufficient angular momentum that its outer parts are unable to collapse and instead form the accretion disc. However, the presence of strong stellar winds in the Wolf-Rayet stars that lead to type Ib/c supernovae would be expected to brake the rotation of the stars and spin them down. A number of possibilities have been considered to overcome this problem. For single stars, the most promising option is low metallicity, which then leads to chemically homogeneous evolution of rapidly-rotating stars (e.g. Yoon & Langer 2005). The low metallicity suppresses stellar mass loss and thus prevents wind-driven spin-down. However, more recent observational evidence suggests that a significant fraction of LGRBs form in higher-metallicity environments where this mechanism

\* email: ross@astro.lu.se

is not plausible (e.g. Levesque et al. 2010; Svensson et al. 2012).

Models proposed for the formation of gamma-ray bursts at higher metallicities mostly focus on exploiting the reservoir of angular momentum stored in the orbit of a binary stellar system in order to provide the spin of the exploding star. Here we focus on angular momentum transfer by tidal interaction (Podsiadlowski et al. 2004; Izzard et al. 2004; Levan et al. 2006). In this scenario, tidal locking of the progenitor core with a massive black-hole companion in the latest stages of its evolution spins the core up to rapid rotation rates. In Section 2 we use the BSE stellar population synthesis code to demonstrate the viability of this pathway and measure its frequency. We then analyse the effects of the binary companion on the accretion rate in the subsequent LGRB, in an attempt to confront this model with the observational data. In Section 3 we describe our model, and in Section 4 our results. Section 5 contains a comparison with observed long-duration gamma-ray bursts, and Section 6 a summary.

## 2 BINARY POPULATION

To obtain a representative population of systems we synthesise a population of BH–BH binaries, utilising the rapid binary population synthesis code BSE (Hurley et al. 2002) with the modifications of Church et al. (2011) which for convenience we summarise here. We have modified BSE following Belczynski et al. (2002) and Belczynski et al. (2008) to include a more realistic prescription for compact object masses, hypercritical accretion during common envelope evolution, and delayed dynamical instability in mass transfer from helium stars in binaries with a large mass ratio. We distribute stellar masses according to the Kroupa et al. (1993) IMF. Binary semi-major axes are chosen from a distribution flat in  $\log a$  between 1 and  $10^4 R_\odot$ . The initial eccentricities of the binaries have little effect on their evolution and are set equal to 0.1 for all binaries. Neutron stars receive a natal kick chosen from the bimodal distribution of Arzoumanian et al. (2002). We do not apply a kick to black holes upon formation.

### 2.1 Criterion to obtain a tidal-spinup gamma-ray burst

Following Levan et al. (2006), we require that the material at the edge of the stellar core must have sufficient angular momentum to fall back into a disc at a radius outside the last stable orbit. This means that the specific angular momentum  $j$  of material at the edge of a core of mass  $M_c$  must satisfy  $j > \sqrt{6}GM_c/c$ . Taking the core to be rotating as a solid body and be tidally locked to the binary, we apply Kepler’s law to obtain a critical orbital separation  $a_{\text{crit}}$  of

$$a_{\text{crit}} = 7.36 R_\odot \left( \frac{M_c}{1.7 M_\odot} \right)^{-2/3} \left( \frac{M_T}{20 M_\odot} \right)^{1/3}, \quad (1)$$

where we have taken a typical core radius for massive stars of  $R_c = 0.2 R_\odot$  and  $M_T$  is the total mass of the binary at this point. For binaries that satisfy this criterion we assume that tidal locking takes place at the point where the orbital

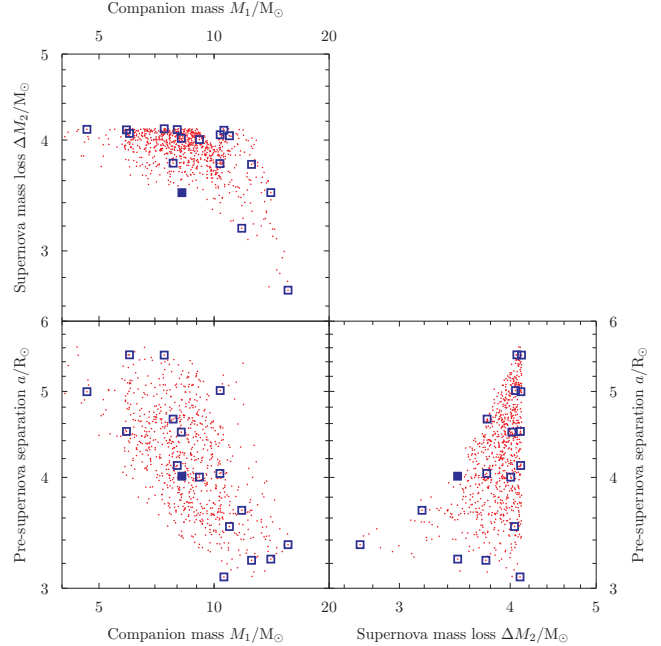


**Figure 1.** The population of binaries that we expect to produce tidal spin-up gamma-ray bursts. In the bottom-left panel we plot the mass of the companion black hole,  $M_1$ , against the binary separation before the second supernova,  $a$ . The top-left panel shows the mass lost in the supernova,  $\Delta M_2$ , against  $M_1$ . The lower-right panel shows  $a$  against  $\Delta M_2$ . In BSE  $\Delta M_2$  is a function of  $M_2$  only. Red dots show all the binaries produced by our population synthesis. Blue squares show the subset of 17 representative systems that we chose to investigate and the filled blue square shows the location of our typical system.

separation is minimised. This gives the specific angular momentum of the material at the edge of the core as

$$j_{\text{shell}} = 6.97 \times 10^6 \text{ km}^2 \text{ s}^{-1} \sqrt{\frac{M_T}{20 M_\odot}} \left( \frac{a_{\text{min}}}{3 R_\odot} \right)^{-3/2}. \quad (2)$$

For cores that match this criterion, the material further inside the core also acquires a substantial angular momentum. The black hole that forms from such a core will have a dimensionless spin parameter close to unity. This makes it a good candidate for powering a long gamma-ray burst via the mechanism of Blandford & Znajek (1977).

### 2.2 Derived population

The population of binaries that we obtain from our BSE runs is shown in Figure 1. We plot the relationships between the companion mass,  $M_1$ , the pre-supernova binary semi-major axis,  $a$ , and the mass lost by the exploding star,  $\Delta M_2$ . The binaries where the criteria for a tidal-spinup LGRB are satisfied are marked with red dots. We choose a sub-sample of 17 systems that cover the parameter space evenly to investigate further; these are marked with blue squares.

To calculate a representative rate for these systems we adopt the approach of Podsiadlowski et al. (2004), along with their rates for LGRBs and core-collapse supernovae in a typical galaxy. We present the rates for our binaries in Table 1. To calculate our rates we employ a Kroupa et al.

Object	Rate yr <sup>-1</sup> /galaxy
Core-collapse supernovae	$7 \times 10^{-3}$
Gamma-ray bursts (beaming angle of 5°)	$3 \times 10^{-5}$
Tidal spin-up LGRBs (conservative estimate)	$2.6 \times 10^{-9}$
Tidal spin-up LGRBs (optimistic estimate)	$1.2 \times 10^{-6}$

**Table 1.** Estimated event rates for a typical galaxy. Values for core-collapse supernovae and gamma-ray bursts are taken from Podsiadlowski et al. (2004).

(1993) IMF and a minimum mass for a core-collapse supernova of  $8 M_{\odot}$ . Our conservative estimate takes a binary fraction of 0.5 for all stars and assumes that their masses are drawn independently from the IMF. The more optimistic estimate – which in our judgement is more realistic – takes the binary fraction to be unity for massive stars and employs a distribution of mass ratios  $f(q) = 2q$ , which biases the sample towards equal-mass binaries.

Our rates, taken at face value, are quite small; even the optimistic estimate is lower than the LGRB rate. This is relatively unsurprising; we require a binary that forms two black holes, one of them rather massive, in a binary with an unusual configuration. It is perhaps unsurprising that such binaries are relatively rare compared to, for example, NS–NS binaries. However, as we show, making a simple change to the mass-ratio distribution in the binary can make a very large difference to the predicted rate. We have not explored further any of the uncertainties in our assumptions about the binary evolution and how they might affect the population of binaries produced, but we are confident that, were we to do so, we would be able to match the observed GRB rate using reasonable assumptions. For example, the number of sufficiently spun-up binaries that we produce is rather sensitive to our assumptions about the radius of the helium core at the closest point in the evolution. We have also not evaluated whether the injection of angular momentum into the fallback material by interaction with a companion can increase the population of binaries with sufficient angular momentum to form a disc. There are also potentially other possible routes to making gamma-ray bursts via tidal spin-up that we have not considered. For example, Moreno Méndez et al. (2011) show that the high spin of black holes in two Galactic binaries is consistent with them being the relics of gamma-ray bursts, as predicted by Lee et al. (2002). Such binaries are likely to be relatively common compared to the massive double black hole binaries that we consider here.

### 2.3 The effects of natal kicks

There is some evidence that black holes receive natal kicks (e.g. Brandt et al. 1995; Gualandris et al. 2005, see also Repetto et al. submitted). To investigate the likely effect of natal kicks on the processes that we are modelling we consider the effect of a moderate kick –  $100 \text{ km s}^{-1}$  – in the four directions in the orbital plane:  $\pm\{x, y\}$ . We do not consider kicks in the  $z$  direction because this breaks the symmetry of the problem about the orbital plane, and hence evaluating the behaviour of the subsequent accretion flow is more complex. In each case we assume that the material that is ejected

and subsequently falls back on to the black hole receives the same kick as the newly-formed black hole itself. This is the expected behaviour if the kick is caused by a mechanism intrinsic to the supernova explosion, which previous work has found to be the most likely case for the Galactic black-hole binary Cygnus X-1 (Axelsson et al. 2011).

## 3 MODELLING THE FALLBACK PROCESS

To treat the fallback process we utilise the simulations of MacFadyen et al. (2001). They find a broadly self-similar behaviour of the accretion of material on to the nascent black hole, with an early plateau phase followed by the  $t^{-5/3}$  decline of Chevalier (1989). We fit this with a two-piece solution:

$$\dot{M} = \begin{cases} \kappa & 100 \text{ s} < t < t_{\text{plateau}} \\ \kappa(t/t_{\text{plateau}})^{-5/3} & t > t_{\text{plateau}} \end{cases} \quad (3)$$

where  $\log_{10}(t_{\text{plateau}} - 100 \text{ s}) = 2.2$ ; i.e.  $t_{\text{plateau}} \simeq 260 \text{ s}$ , and  $\kappa$  is chosen to obtain the correct total fallback mass. To obtain the fallback mass we assume that the inner  $2 M_{\odot}$  of the final black hole mass is acquired during the initial core collapse; the remainder forms the fallback mass. This prescription leads to a fallback mass of between 1 and  $3 M_{\odot}$ .

### 3.1 Particle trajectories

By using the results of hydrodynamic simulations of black-hole formation in fallback supernovae in the form of Equation 3 we avoid having to compute the hydrodynamics of the accretion shocks ourselves. Instead we treat our particles as interacting only under gravity. We launch our particles with a distribution of velocities, chosen so that, in the absence of a companion star, the particles would fall back with times that reproduce the accretion rate given by Equation 3. For purely radial motion the return time  $t_{\text{return}}$  for a particle launched at radius  $r_0$  from a star of mass  $M_i$  is given by

$$t_{\text{return}} = \sqrt{\frac{r_0^3}{GM_i}} \left( \frac{\alpha}{1-\alpha} \right) \left( \alpha + \sqrt{\frac{\alpha}{1-\alpha}} \tan^{-1} \sqrt{\frac{\alpha}{1-\alpha}} \right), \quad (4)$$

where  $\alpha$  is related to the particle's launch velocity  $v_0$  according to

$$v_0 = \sqrt{\alpha \frac{2GM_i}{r_0}}. \quad (5)$$

We invert Equation 4 numerically in order to produce a distribution of  $\alpha$  from the accretion rate of Equation 3. Because the star is rotating the initial velocities are not radial; however, because  $r_0$  is small compared to the maximum distance that the particle reaches from the exploding star, Equation 4 suffices. We choose the value of  $r_0$  so that the rotational velocity at the equator is 20% of the escape velocity at that radius; thus even at launch the particle velocities are predominantly radial.

We follow the motion of the particles under the gravitational force of the two black holes. As we are using Equation 3 to account for the self-interaction of the gas we ignore the mass of the gas particles and any non-gravitational forces; in practice, therefore, we solve the reduced three-body problem numerically. We use the Bulirsch-

Stoer method as given by Press et al. (1992) to integrate the orbits of the stars and particles.

We follow the motion of the particles until they cross the orbital plane ( $z = 0$ ) for the first time. The angular momentum vector of the stellar rotation is parallel to that of the orbit as it is induced by tidal spin-up of the exploding star: hence the system is symmetric under reflection in the orbital plane. Because we can expect any given particle that crosses the orbital plane to have a counterpart with the equal and opposite  $z$ -velocity a disc will form in the plane. We measure the mass and momentum flows into the disc by monitoring the rate at which particles cross the plane and the specific angular momentum that they possess when they do. We assume that any particles that cross the plane sufficiently close to a black hole to be within the last stable orbit are accreted directly.

### 3.2 Accretion disc

Following Perna et al. (2006) we use a simple treatment of the accretion disc based on the viscous timescale. We assume that a ring of material, represented by one of our particles that has accreted into the  $x - y$  plane, will move inward through the disc via viscous dissipation of angular momentum. The rate at which a particle moves inward is given by

$$\frac{dr}{dt} = -\frac{r}{t_0}, \quad (6)$$

with characteristic viscous timescale  $t_0$  given by

$$t_0 = \left( \frac{R_{\text{disc}}}{H_{\text{disc}}} \right)^2 \frac{1}{\alpha \Omega_{\text{Kep}}} \quad (7)$$

for a disc of scale height  $H$  and radius  $R$ . The orbital angular frequency at radius  $r$  in the disc around the compact object with mass  $M_i$  is given by

$$\Omega_{\text{Kep}} = \sqrt{\frac{GM_i}{r^3}}. \quad (8)$$

We take the ratio  $R_{\text{disc}}/H_{\text{disc}} = 10$  to be fixed throughout the evolution. Although the disc is probably less flat than this at early times the viscous timescale then is short enough for the results to be basically unaffected. A particle unaffected by other particles, arriving at the disc at time  $\tau$ , then spirals towards the central black hole according to

$$r(t) = r(\tau) \left[ 1 - \frac{3}{2} \frac{t - \tau}{t_0(\tau)} \right]^{2/3}. \quad (9)$$

We set  $r(\tau)$  to be the particle's circularisation radius; that is, we assume that the material that it represents will self-collide to form a circular ring, conserving specific angular momentum. Thus the initial radius at which the particle joins the disc is given, in terms of its specific angular momentum  $j$ , by

$$r(\tau) = r_{\text{circ}} = \frac{j^2}{GM_i}. \quad (10)$$

In the process of circularising, i.e. moving between the radius from the central object at which it enters the plane and that at which it circularises, the material may collide with gas already present in the disc. If this happens we merge the two colliding particles and calculate a new specific angular

momentum, and hence circularisation radius. This process is repeated until the particle has successfully circularised. Particles that circularise outside the instantaneous Roche lobe of either star are assumed to be lost from the system. We have tested that the accretion history resulting from this treatment converges as we increase the number of particles, and hence the mass resolution of the simulation.

## 4 RESULTS

We present first the results for a typical binary, indicated by the filled square in Figure 1. It has a companion black-hole mass of  $M_1 = 8.24 M_\odot$ ; the newly-formed black hole has a total mass, including the material falling back, of  $M_2 = 4.29 M_\odot$ , having lost  $\Delta M_2 = 3.49 M_\odot$  in the explosion. The semi-major axis of the orbit at the time of explosion is  $a = 4.01 R_\odot$ .

In Figure 2 we plot the location of each particle in the simulation when it crosses the orbital plane. The exploding star is initially moving in the  $+y$  direction. As it proceeds round its orbit, the particles that fall back towards it have been affected to a greater degree by interaction with the companion, so their deviation from the stellar position is increased. These particles typically also have more specific angular momentum and hence enter the accretion disc at larger radii. After a some time – about one quarter of the post-explosion orbital period of the binary – the particles start to mostly fall back outside the Roche lobe of the star and hence the mass inflow rate into the disc reduces sharply. Some particles instead, however, fall into the Roche lobe of the companion black hole (blue dots in Figure 2). The accretion rate on to the two stars as a function of time in this typical model is shown in Figure 3.

Our typical model shows a number of features that are common to the models that we have run. There is an initial plateau followed by a declining power-law accretion rate. This follows directly from our input accretion rate; the particles falling back at early times are largely unaffected by the presence of the companion. At roughly  $10^4$  s there is a break in the accretion curve, which transitions to a steeper power law. Finally there is a period of zero accretion at about  $1.75 \times 10^4$  s, followed by a flare that lasts for several  $10^4$  s. During this flare there is additionally some accretion on to the companion black hole.

### 4.1 Fits to the accretion behaviour

To gain some insight into the implications of our model we fit each of our 17 characteristic systems with a broken power-law model of the form

$$\dot{M} \propto \begin{cases} t^{\gamma_1} & 200 \text{ s} < t < t_{\text{break}} \\ t^{\gamma_2} & t_{\text{break}} < t < t_0, \end{cases} \quad (11)$$

where  $\gamma_1$ ,  $\gamma_2$  and  $t_{\text{break}}$  are obtained by fitting. The time at which the accretion first ceases,  $t_0$ , is obtained from the accretion curve. In Figure 4 we present the results of the fits. The bottom-left panel shows the break time,  $t_{\text{break}}$ , plotted as a function of  $\gamma_1$ , the power-law index of the portion of the accretion curve before the break. The plot shows that the accretion curves are somewhat steeper than the  $t^{-5/3}$  input power-law; shorter break times are correlated with more

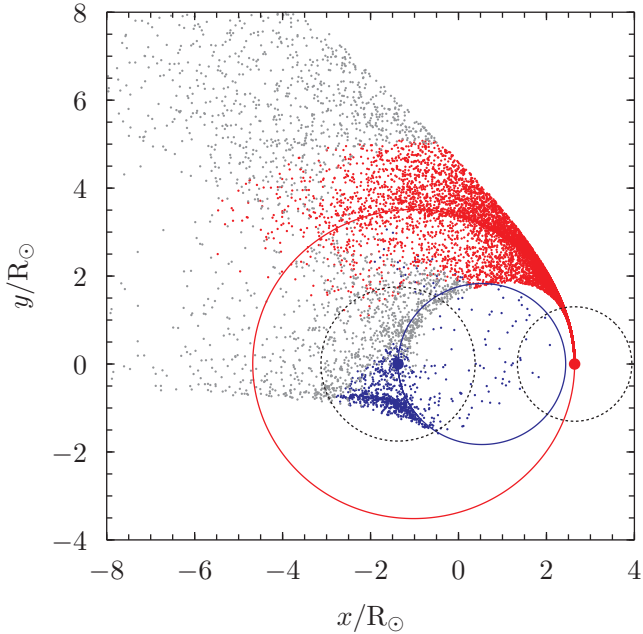


**Figure 2.** The locations where particles cross the orbital plane in our reference simulation. The large red and blue points are the initial positions of the exploding star and companion black hole respectively. The red and blue solid lines show the post-supernova orbits of the two stars. Initially the exploding (red) star is moving in the  $+y$  direction and the companion black hole (blue) in the  $-y$  direction. The red dots are particles that fall into a disc around the newly-formed black hole; similarly, the blue dots are particles that fall into a disc around the companion black hole. Grey dots are particles that fall further from either object than its Roche lobe radius and hence are expected not to be accreted. The black dashed lines show the initial radii of the Roche lobes around the two stars. The origin of the co-ordinate system is the centre of mass of the post-explosion system. For clarity only 1% of the particles used in the final simulation are plotted.

steeply declining accretion. The power-law index of the second, post-break power law segment is much steeper, typically between  $-5$  and  $-10$ , and does not show any correlation with the other parameters.

In Figure 5 we present the correlation between the semi-major axis of the binary,  $a$ , and the accretion break time. The evident correlation has a simple explanation; a wider orbit means that the material has to travel further before it interacts significantly with the companion black hole, increasing  $t_{\text{break}}$ . This in turn also means that the angular momentum imparted to the material which is accreted before the break is lessened; hence there is a positive correlation between  $a$  and  $\gamma_1$ .

In both Figures 4 and 5 we plot both systems computed under the assumption of black-hole kicks, as well as unknicked systems. We find that the behaviour of the kicked and unknicked systems is broadly similar to the unknicked case, and there are no marked trends between the different kicks. This suggests that a moderate kick is unlikely to have a strong effect on the fallback process.

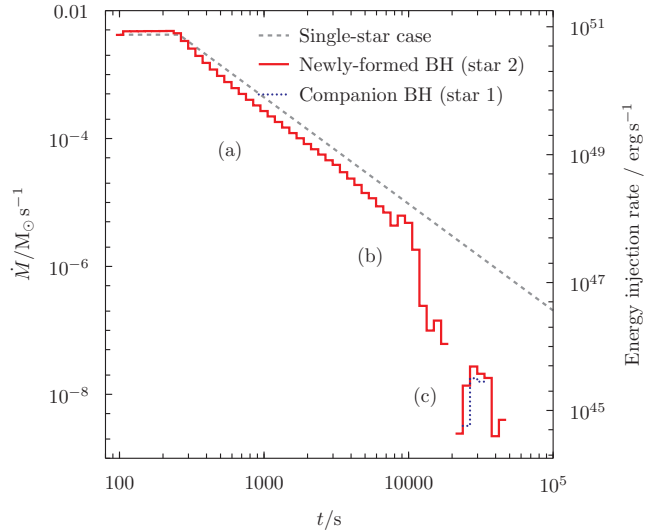


**Figure 3.** The accretion rate on to the black holes in our typical example system. The grey dashed line shows the accretion rate of Equation 3, which would be obtained in the absence of a companion. The red solid line shows accretion on to the newly-formed black hole (star 2) whilst the blue dotted line is for the companion (star 1). The plot includes the effect of the accretion disc and the Roche lobes of the two stars. Of the  $2.29 M_{\odot}$  of material in the fallback shell  $1.90 M_{\odot}$  is accreted on to star 2 and  $0.02 M_{\odot}$  on to star 1; the remaining  $0.37 M_{\odot}$  is lost from the system. Characteristic features are (a) the initial plateau and roughly  $t^{-5/3}$  decline phases, (b) the break in the accretion rate at roughly  $10^4$  s followed by a steep decline, and (c) some late-time accretion activity (at around  $3 \times 10^4$  s). The right-hand axis shows the energy injection from accretion, assuming that the efficiency of conversion of mass to energy is  $\eta = 0.1$ .

## 5 COMPARISON WITH OBSERVATIONS

It is difficult to compare our results directly with observations. In order to go from the black hole's accretion history to the observed photometry and spectral features it is necessary to model the propagation of the fireball and jet through the exploding star, a highly involved procedure. What we can say, however, is that we expect to see evidence of continued energy injection during the first approximately  $10^4$  s in the rest frame of the accreting black hole. We predict that the rate of this energy injection would decline quite strongly, although we should caution against the use of our fitted values of  $\gamma$  as the decline of the injected luminosity. As the system evolves and the accretion rate decreases the accretion morphology will become more disc-like and less advection dominated. This will increase the fraction of the accretion luminosity available to power a jet at later times.

Secondly, we predict a sharp reduction in the accretion luminosity at times of around  $10^4$  s, which we would expect to appear as a break in the light curve. These times are consistent with typical times found by Evans et al. (2009) for the end of the plateau phase in canonical light curves, whose distribution also peaks at about  $10^4$  s. Light curves that show a single, steepening break also have break times around  $10^4$  s, although the distribution is much wider. Our break times are also consistent with the subset of the sample of light curves presented by Li et al. (2012) that show shallow decay features. Interpretation of the optical light curves

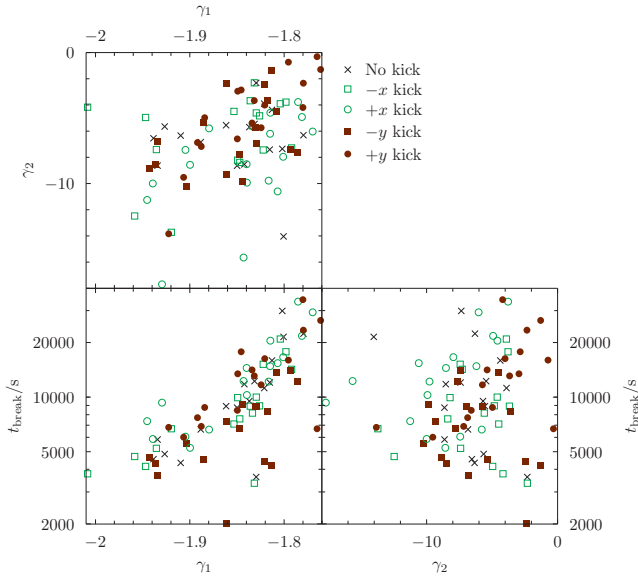


**Figure 4.** Correlations between different parameters in our power-law fits to the accretion rates on to the two black holes. The power-law applicable to the decay between 200 s and the break time  $t_{\text{break}}$  is denoted by  $\gamma_1$ , whereas the power law between  $t_{\text{break}}$  and the first cessation of accretion is denoted by  $\gamma_2$ . The bottom-left panel shows the correlation between  $\gamma_1$  and  $t_{\text{break}}$ , the top-left panel that between  $\gamma_1$  and  $\gamma_2$ , and the bottom-right panel that between  $\gamma_2$  and  $t_{\text{break}}$ . Black crosses are for models without natal kicks, brown filled circles and squares are models with kicks in the  $+y$  and  $-y$  directions, and green open circles and squares are models with kicks in the  $+x$  and  $-x$  directions. Only the first of these three shows a significant correlation.

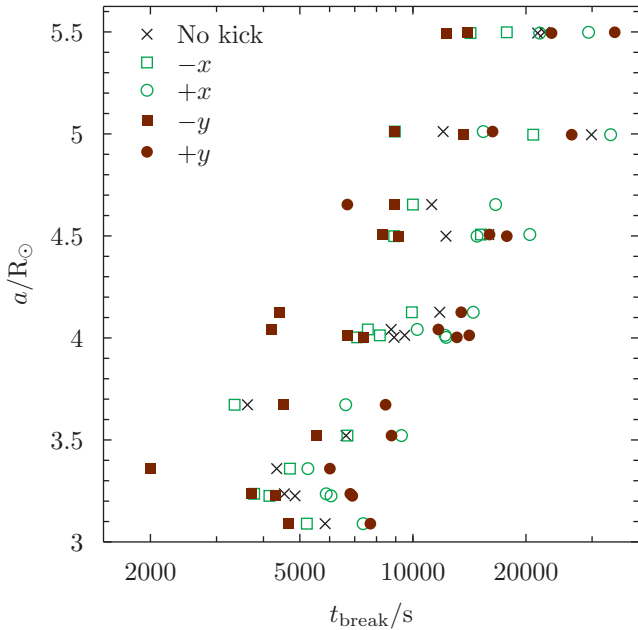


**Figure 5.** The correlation between the binary semi-major axis  $a$  and the break time  $t_{\text{break}}$ . Wider binaries only affect particles falling back at later times, thus making  $t_{\text{break}}$  later for larger semi-major axis. Black crosses are for models without natal kicks, brown filled circles and squares are models with kicks in the  $+y$  and  $-y$  directions, and green open circles and squares are models with kicks in the  $+x$  and  $-x$  directions.

is complicated, however, by spectral breaks which can occur at relevantly late times.

The physical origin of the break in our models is the truncation of accretion by the Roche lobe of the exploding star. Material that falls outside the Roche lobe is not bound to either star, and hence will be lost from the system. As time progresses, the material falling back has traversed a larger distance from the exploding star and hence is more affected by the gravitational force of the companion. Thus it falls back at a greater distance from the exploding star. The break time can be understood as the time at which this distance is the Roche lobe radius of the star. This is the origin of the correlation visible in Figure 5, as in wider binaries the Roche lobe is larger and thus the break time is later.

### 5.1 Late-time highly-variable accretion

The majority of our models include some form of late-time highly-variable accretion. This typically occurs at a few times  $t_{\text{break}}$ , after the second power-law component has ended. In our typical system, for example, after the main accretion episode has ended at around  $2 \times 10^4$  s there is a renewed episode of accretion peaking at around  $3 \times 10^4$  s. Such activity might power late-time flares. In Figure 6 we show the properties of the flares in those of our models that show them. We assume that, once the accretion energy conversion efficiency has been taken into account, all the energy liberated goes into the flare. Having done this, the luminosity generated is very comparable to that seen in late-time flares observed in the X-ray and optical. For comparison, we plot the energy in the late-time flares of three observed long gamma-ray bursts, GRB 050502B, GRB 070107 and GRB 070318. This is the subset of the sample considered by Curran et al. (2008) that have reasonably constrained photometric or spectroscopic redshifts and which are long bursts. We take the light curves for these flares from Evans et al. (2009) and redshifts from Xiao & Schaefer (2011). Although the observed flares appear to be somewhat more energetic than our predictions, it is only necessary for them to be beamed to one tenth of the sky at the time of the flare to be consistent with our predicted values. We re-produce the observed decline in flare energy with time, which is also seen in optical data (Li et al. 2012).

## 6 DISCUSSION

We have considered tidal spin-up compact binaries as a possible source for long-duration gamma-ray bursts. We show that, with appropriate assumptions, a population synthesis approach predicts that these binaries will be produced. Furthermore we show that, given two different – but plausible – assumptions about the distribution of mass-ratios of high-mass binaries we predict two very different formation rates. Hence we suggest that the power of population synthesis calculations to constrain progenitor models by analysis of expected rates is rather weak, as argued by Tout (2005) for the similar problem of Type Ia supernova progenitors.

A potential means of distinguishing this progenitor scenario, however, is that in the case of a tidally spun-up progenitor, the star exploding as a type Ib/c supernova has

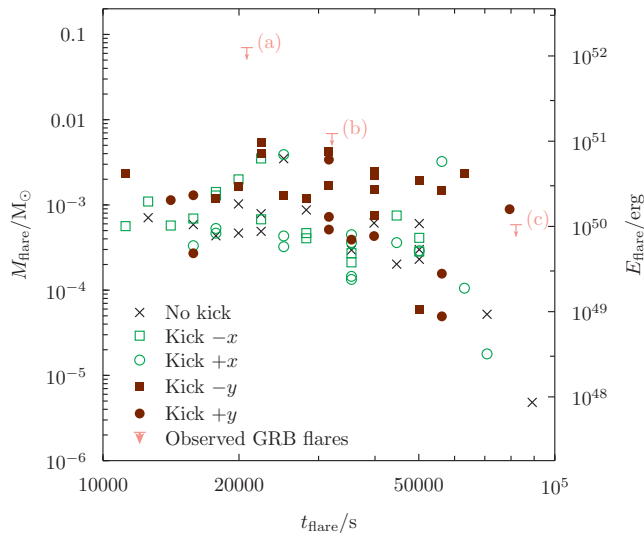


**Figure 6.** Episodes of highly-variable late-time accretion in our models. We plot the total mass accreted in late-time flares,  $M_{\text{flare}}$ , as a function of the break time  $t_{\text{break}}$ . As in previous figures, black points are for models without natal kicks, brown filled circles and squares are models with kicks in the  $+y$  and  $-y$  directions, and green open circles squares are models with kicks in the  $+x$  and  $-x$  directions. Flare energies (right-hand axis) are calculated assuming mass is converted into energy with an efficiency of  $\eta = 0.1$ . The pink upper limits represent the energy in late-time flares from three long-duration gamma-ray bursts, (a) GRB 050502B, (b) GRB 070107 and (c) GRB 070318. In calculating these points we assume that the energy emission at the time of the flare is isotropic.

a black-hole companion. We have modelled the effect of the companion on the fallback process to investigate what observable consequences it would have for the gamma-ray burst. We conclude that our models possess the following general features:

- Before about  $10^4$  s, an accretion rate onto the newly-formed black hole that declines as  $t^{-1.85 \pm 0.05}$ ,
- a break in the accretion rate at around  $10^4$  s, with a steeply declining accretion rate thereafter, and
- in the majority of cases, highly-variable late-time accretion, leading to flares at times between  $10^4$  and  $10^5$  s, of total energies around  $10^{50}$  erg.

These general features are broadly consistent with the observations of long-duration gamma-ray bursts. Bursts with a canonical-type light curve show evidence of energy injection up until roughly the times that we predict, with a break thereafter. For the three bursts from the sample of Curran et al. (2008) that have a well-defined redshift and late-time bursts, the properties of the bursts agree with our predictions, assuming a reasonable beaming fraction. We reproduce the tentative correlation between the time of the flare and the energy. We caution, however, that our model on its own cannot explain flares that occur prior to  $10^4$  s. It does not preclude such flares from occurring; however, they must have a separate origin, such as instabilities in the accretion flow onto the newly-formed black hole.

Although we have only considered tidal spin-up by a massive compact companion, it is also possible that the exploding star could be spun up by a main-sequence compan-

ion. Lee et al. (2002) consider the evolution of the progenitors of low-mass X-ray binaries. They show that tidal forces from a low-mass main-sequence companion and frictional effects during common-envelope evolution can be sufficient to spin up the outer layers of the helium star, which subsequently collapses to give a black hole. We expect gamma-ray bursts produced by such a system to also show breaks and flares similar to those described in this paper; the binary has a similar semi-major axis and the same processes will operate. We intend to undertake a quantitative study of these binaries in a subsequent work.

Finally, we investigate the effect of black-hole kicks on our scenario and show that a moderate kick is expected to have a relatively small effect on the observed properties of the burst. We caution, however, that our model can only encompass kicks that are directed within the orbital plane of the binary. Kicks with a component parallel to the angular momentum vector would disturb the geometry of the situation; this could make the accretion flow more disc-like and less spherical, which we would expect to have significant consequences for the baryon loading of the resulting burst.

## ACKNOWLEDGEMENTS

The authors would like to thank Johan Fynbo for useful discussions. RPC is funded by a Marie-Curie Intra-European Fellowship, grant No. 252431, under the European Commission's FP7 framework. CK acknowledges a Marie-Curie International Incoming Fellowship under the European Commission's FP7 framework. This work was supported by the Swedish Research Council (grants 2008-4089 and 2011-3991). The calculations presented in this paper were carried out using computer hardware purchased with grants from the Royal Fysiographic Society of Lund. This work made use of data supplied by the UK Swift Science Data Centre at the University of Leicester.

## REFERENCES

- Arzoumanian, Z., Chernoff, D. F., Cordes, J. M., 2002, *ApJ*, 568, 289
- Axelsson, M., Church, R. P., Davies, M. B., Levan, A. J., Ryde, F., 2011, *MNRAS*, 412, 2260
- Belczynski, K., Kalogera, V., Bulik, T., 2002, *ApJ*, 572, 407
- Belczynski, K., Kalogera, V., Rasio, F. A., Taam, R. E., Zezas, A., Bulik, T., Maccarone, T. J., Ivanova, N., 2008, *ApJS*, 174, 223
- Blandford, R. D., Znajek, R. L., 1977, *MNRAS*, 179, 433
- Brandt, W. N., Podsiadlowski, P., Sigurdsson, S., 1995, *MNRAS*, 277, L35
- Chevalier, R. A., 1989, *ApJ*, 346, 847
- Church, R. P., Levan, A. J., Davies, M. B., Tanvir, N., 2011, *MNRAS*, 413, 2004
- Curran, P. A., Starling, R. L. C., O'Brien, P. T., Godet, O., van der Horst, A. J., Wijers, R. A. M. J., 2008, *A&A*, 487, 533
- Evans, P. A., et al., 2009, *MNRAS*, 397, 1177
- Gehrels, N., et al., 2004, *ApJ*, 611, 1005

- Gualandris, A., Colpi, M., Portegies Zwart, S., Possenti, A., 2005, *ApJ*, 618, 845
- Hjorth, J., Bloom, J. S., 2011, [astro-ph/1104.2274](#)
- Hurley, J. R., Tout, C. A., Pols, O. R., 2002, *MNRAS*, 329, 897
- Izzard, R. G., Ramirez-Ruiz, E., Tout, C. A., 2004, *MNRAS*, 348, 1215
- Kroupa, P., Tout, C. A., Gilmore, G., 1993, *MNRAS*, 262, 545
- Lee, C.-H., Brown, G. E., Wijers, R. A. M. J., 2002, *ApJ*, 575, 996
- Levan, A. J., Davies, M. B., King, A. R., 2006, *MNRAS*, 372, 1351
- Levesque, E. M., Kewley, L. J., Graham, J. F., Fruchter, A. S., 2010, *ApJ*, 712, L26
- Li, L., et al., 2012, [astro-ph/1203.2332](#)
- MacFadyen, A. I., Woosley, S. E., Heger, A., 2001, *ApJ*, 550, 410
- Moreno Méndez, E., Brown, G. E., Lee, C.-H., Walter, F. M., 2011, *ApJ*, 727, 29
- Perna, R., Armitage, P. J., Zhang, B., 2006, *ApJ*, 636, L29
- Podsiadlowski, P., Mazzali, P. A., Nomoto, K., Lazzati, D., Cappellaro, E., 2004, *ApJ*, 607, L17
- Press, W. H., Teukolsky, S. A., Vetterling, W. T., Flannery, B. P., 1992, *Numerical recipes in FORTRAN. The art of scientific computing*
- Repetto, S., Davies, M. B., Sigurdsson, S., 2012, [astro-ph/1203.3077](#)
- Stanek, K. Z., et al., 2003, *ApJ*, 591, L17
- Svensson, K. M., et al., 2012, *MNRAS*, 421, 25
- Tout, C. A., 2005, in J.-M. Hameury & J.-P. Lasota, ed., *The Astrophysics of Cataclysmic Variables and Related Objects*, vol. 330 of *Astronomical Society of the Pacific Conference Series*, p. 279
- Woosley, S. E., 1993, *ApJ*, 405, 273
- Xiao, L., Schaefer, B. E., 2011, *ApJ*, 731, 103
- Yoon, S.-C., Langer, N., 2005, *A&A*, 443, 643